Diagnostics for advanced materials processing by plasma spraying*

C. Moreau‡, J.-F. Bisson†, R. S. Lima, and B. R. Marple

National Research Council Canada, Industrial Materials Institute, 75 de Mortagne, Boucherville (Québec), J4B 6Y4, Canada

Abstract: Advanced coatings deposited by plasma spraying are used in a large variety of industrial applications. The sprayed coatings are employed typically in industry to protect parts from severe operating conditions or to produce surfaces with specific functions. Applications are found in many industrial sectors such as aerospace, automobile, energy generation, and biomedical implants.

Coatings are built by the successive deposition of molten or partially molten particles that flatten and solidify upon contact on the substrate, forming lamellae. The coating properties are intimately linked to the properties of these lamellae, which in turn depend on in-flight particle properties as well as substrate temperature during spraying. Consequently, the development of diagnostic tools for monitoring and controlling these spray parameters will help provide the necessary information to study the coating formation process, optimize the coating properties, and, eventually, control the spray process in production.

In this paper, a review of some recent developments of optical diagnostic techniques applied to monitor plasma-sprayed particles is presented. In the first part of the paper, two different sensing techniques for in-flight particle measurement are described. First, time-resolved diagnostics on individual particles is described. This technique is used to study the instabilities of the particle characteristics associated with the plasma fluctuations. Secondly, a technique adapted for use in an industrial production environment for measuring the particle jet characteristics as an ensemble is presented. In the second part of the paper, the use of an optical system to study the influence of the substrate temperature on the flattening and solidification of sprayed particles impacting on a flat substrate is described. The last part of this paper describes the optimization of nanostructured coatings based on a tight control of the temperature and velocity of the plasma-sprayed particles.

Keywords: particle diagnostics; plasma spraying; optical sensors; particle flattening; nanostructured coatings.

INTRODUCTION

Plasma spraying is a process widely used in industry for depositing protective and functional coatings for a large variety of applications. Industrial sectors such as aerospace, automotive, energy, mining, biomedical, etc. take advantage of the unique properties of the sprayed coatings [1]. The versatility of this

process allows the deposition of ceramics, metals, polymers, and composite materials on substrates of different sizes, ranging from millimetre-long dental implants to kilometre-long bridges. The development of this technology over the last 40 years was initially carried out in an empirical manner. Varying input spray parameters such as current, gas flow rates, etc. and evaluating the coating characteristics and performance in specific applications developed coatings. Major advances were achieved by this approach, permitting the development of efficient coatings for a broad spectrum of applications.

However, to push the technology to the next level, it was necessary to develop a better understanding of the different processing steps involved in spray deposition as well as a deeper knowledge of the characteristics of the coatings required for specific applications. That is to say, an important research effort was dedicated to the study of the plasma formation, heat and momentum transfer to the particles, coating build-up, and coating property characterization as described recently by Fauchais et al. [2]. This intensive research effort permitted changing paradigms for further developing the technology from a trial-and-error approach to a more scientific approach, from an art to a science.

In order to progress toward this direction, it is mandatory to develop diagnostics tools that give researchers the necessary data to understand the physical, chemical, and metallurgical processes involved during plasma spraying. This is a challenging task as the plasma spray process involves extreme temperatures, temperature gradients, and instabilities in the plasma flow as well as rapid changes in the temperature and velocity of the sprayed particles, especially upon impact on the substrate surface. Another important challenge relates to the stability of the plasma spraying process. Indeed, many factors affect the plasma characteristics and the heat and momentum transfers to the particles. Particle temperature and velocity have a profound effect on the coating characteristics and are very sensitive to minute changes in the electrode position, electrode surface condition, injector geometry, etc. [3–5]. This high sensitivity makes the process very difficult to control, although all input spray parameters (for example, plasma current, primary and secondary gas flow rates, powder feed rate) are well under control. Adapted diagnostic tools are also required to monitor and control the state of key parameters in production for ensuring the deposition of consistent and reliable coatings [6,7].

In recent years, many new diagnostic tools have been developed for addressing these two important needs: better understanding of the different processing steps and better control of the plasma spray process. A lot of effort has been dedicated to these areas, especially to the development of diagnostics tools for in-flight particle monitoring. This work was initiated mostly in research laboratories in France, the United States, Canada, and Russia and triggered the development of new commercial sensors that are now available [8–13]. For example, diagnostic equipment based on using two-color pyrometry and time-of-flight techniques is available for use in both a research environment and in industrial facilities [14–16]. Monitoring devices based on rapid charge-coupled device (CCD) cameras have also been commercialized [17–20]. These sensors are widely used today in many research laboratories and in some industrial spray facilities.

In this paper, recent work on the development and application of particle diagnostics carried out at the authors' institute are presented. The research efforts have focused on optical diagnostic tools for monitoring plasma-sprayed particles in flight and upon impact on a substrate. The paper is structured as follows. In the first part of the paper, diagnostic tools for monitoring in-flight particles are described. First, time-resolved diagnostics on individual particles is described. This technique is used to study the instabilities of the particle characteristics associated with the plasma fluctuations owing to the cyclic movement of the arc root at the anode surface. Particle instabilities are found to affect the coating structure and deposition efficiency. Secondly, a technique for measuring the particle jet characteristics as an ensemble is presented. This approach is adapted for use in an industrial production environment for monitoring and controlling plasma spray processes. In the second part of the paper, an optical system for monitoring plasma spray particles impacting on a substrate is described. Such a system is used to study the influence of substrate temperature on the flattening and solidification of individual particles impacting on flat substrates. Finally, in the last part, practical considerations related to the optimization

and control of the plasma spray process are discussed. The optimization of nanostructured coatings carried out by controlling in-flight particle conditions is given as an example.

MONITORING OF IN-FLIGHT PARTICLES

Developing and using optical sensors for monitoring the condition of in-flight particles is essential for understanding the complex relationships between spray parameters, in-flight particle characteristics, coating microstructure and properties. Moreover, since the coating attributes strongly depend on the particle condition during spraying, the use of optical sensors becomes a practical way to control the plasma spray process in order to get consistent coating properties and optimum deposition efficiency on the production floor. To address the needs of both scientists and engineers, two types of sensors were developed and later commercialized [16]. Both systems detect and analyze the thermal radiation emitted by the hot particles. The first system, now widely known by the trade name DPV-2000, detects individual particles and determines for each particle its temperature, velocity, and diameter. The second system, more recently introduced under the trade name Accuraspray, is dedicated to use on the production floor. It measures the mean temperature and velocity of the particle jet as well as its width, orientation, and intensity.

Monitoring of individual in-flight particles

The DPV-2000 system has been described in detail in previous papers [14,21]. The thermal radiation collected by the sensor head is transmitted to the detection cabinet by an optical fiber. Typically, the sensor head is mounted on an X-Y displacement system for performing 2D mappings across the spray jet. When a particle travels in the field of view of the sensor head, its image is formed on a two-slit mask mounted at the tip of the optical fiber as illustrated in Fig. 1. The collected radiation is detected using two avalanche photo-detectors (D_1 and D_2) filtered at two distinct wavelengths. A two-peak pulse is recorded in each detector when a particle crosses the sensor field of view. The temperature of the particles is calculated from the ratio of the signals detected at the two wavelengths, assuming a gray body behavior. The distance between the two slits of the optical mask and the magnification of the optics being known, the particle velocity is obtained by measuring the time of flight of the particle image from the first to the second slit. The relative diameter of the analyzed particles is computed from the absolute intensity detected at one wavelength after determination of its temperature. This system is employed as a diagnostics tool for coating optimization. An example of such an application is given in the last section of this paper for the optimization of high-performance nanostructured titania coatings.
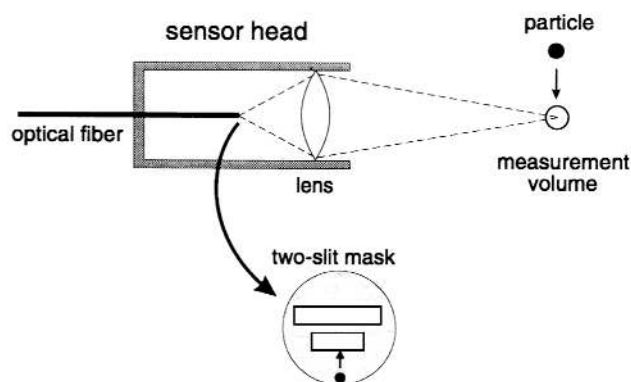

Fig. 1 Schematic view of the sensor head of the DPV-2000 used to monitor the temperature, velocity, and diameter of plasma-sprayed particles.

Recently, the system was used to investigate the influence of the plasma fluctuations on the characteristics of the in-flight particles [22,23]. Plasma fluctuations result from the movement of the arc root on the anode surface driven by the hydrodynamic and electromagnetic forces acting on the arc itself. Different arc behaviors or modes are possible depending on the actual plasma parameters. In particular, the so-called restrike [24,25] mode involves relatively large longitudinal displacements of the arc root leading to important voltage fluctuations while the current is kept constant. Time-resolved particle diagnostics was used to investigate the influence of the plasma fluctuations on spray particle conditions.

Figure 2 shows the voltage signature when a plasma torch was operated in the restrike mode obtained with a relatively low current (550 A) and high hydrogen flow rate (10 l/min). The signal is quasi-periodic with a fundamental frequency of about 4.4 kHz (a period of around 225 µs). To get time-resolved measurements of the particle characteristics, the torch voltage was used as a timing reference for signal acquisition with the DPV-2000. When the voltage reaches a certain level (trigger level), a dedicated electronic circuit generates a pulse after an adjustable time delay. This pulse is used to trigger the signal acquisition by the DPV-2000. The capture time window is adjusted to 20 µs. Then the system analyzes the acquired signals and if one particle was in the field of view of the sensor head during this 20-µs time interval, it determines the temperature, velocity, and diameter of this particle. The acquisition sequence is schematically shown in Fig. 2. Data acquisition continues until about 300 particles are analyzed. Then the time delay is changed for acquiring a new set of data.
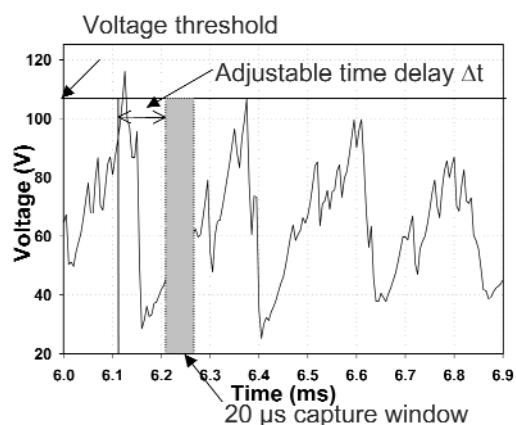

Fig. 2 Voltage fluctuations recorded at the plasma torch. The DPV-2000 acquisition is triggered following a time delay Δt after the voltage exceeds a selected threshold (after ref. [22]).

Alumina particles with a relatively narrow particle size distribution (30 ± 5 µm) were injected in the plasma stream and were detected at 50 mm from the plasma torch exit. Figures 3a and 3b show the measured mean particle temperature and velocity as a function of the time delay. Error bars represent 1σ confidence interval on the mean values, while numerical values are the sample standard deviations. Huge periodic variations of the particle temperature and velocity are observed, reaching 500 °C and 200 m/s, respectively. The period of the cycles coincides with that of the voltage fluctuations as shown in Fig. 2. The magnitude of the fluctuation decreases with the time delay due to the quasi-periodic nature of the plasma and voltage fluctuations. Indeed, the Fourier spectrum of the voltage fluctuation shows that the 4.5 kHz peak has a finesse of about 10. Consequently, the phase reference is lost gradually after a few cycles, leading to a gradual decrease of the amplitude of the temperature and velocity fluctuations as shown in Figs. 3a and 3b.
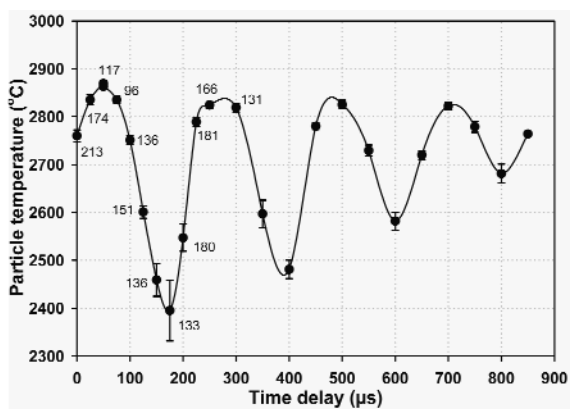
a)
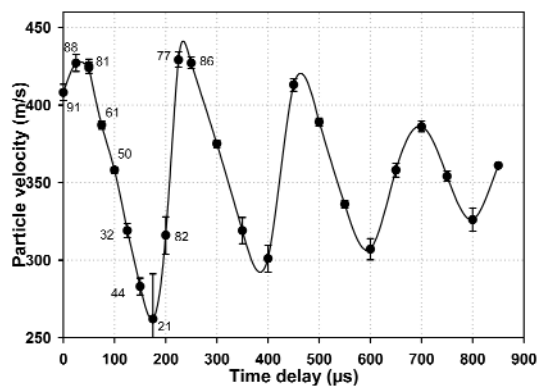
b)

Fig. 3 Time-resolved (a) temperature and (b) velocity measurements of plasma-sprayed alumina particles. Error bars correspond to 1σ confidence on the mean values. Numbers are the sample standard deviations (after ref. [22]).

The plasma fluctuation does not give rise only to periodic fluctuations in the temperature and velocity of the sprayed particles, but also in the particle flow rate as illustrated in Fig. 4. One can see in this figure that the number of detected particles varies by more than one order of magnitude with the
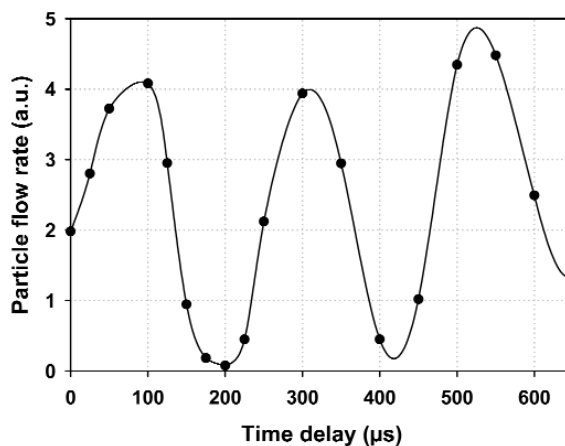

Fig. 4 Time-resolved flow rate measurement of the plasma-sprayed alumina particles. The actual flow rate changed by more than one order of magnitude with the time delay (after ref. [22]).

time delay. This suggests that particles injected into the plasma at certain specific moments are not heated and accelerated efficiently.

To track these unheated or cold particles, a laser diode was used to illuminate the particles in the field of view of the DPV-2000 [23]. In this case, detector D_1 was filtered at the same wavelength, 830 nm, as the laser diode while detector D_2 was filtered at 995 nm. This made it possible to distinguish between "cold" and "hot" particles. Indeed, a cold particle generated a two-peak signal only in detector D_1, while no detectable thermal radiation was collected in detector D_2. Conversely, the thermal radiation emitted by a hot particle generated signals in both detectors. Using this set-up, the velocity and flow rate of the cold particles could be measured when the laser diode was turned on. When the laser was turned off, the temperature, velocity, diameter, and flow rate of the hot particles could be measured as usual with the DPV-2000.

Figure 5 illustrates the velocity fluctuations of both the cold and hot particles observed in spray conditions similar to those described above. Significant fluctuations of the cold particle flow rate are also observed. As expected, the velocity of the cold particles is significantly lower than that of the hot particles and varies also with the time delay. The lower velocity of the cold particles is attributed to their passage in the plasma flame when the enthalpy and thus the gas velocity are minimum. So, the heat and momentum transfer to the particles is also minimum during these periods.
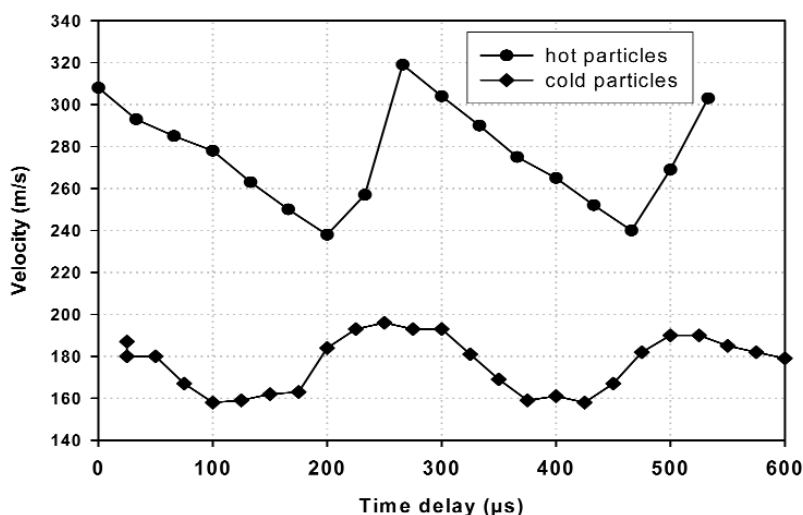

Fig. 5 Time-resolved velocity measurements of "hot" and "cold" alumina plasma-sprayed particles.

Global measurement of particle jet characteristics

Wear of the electrodes with spraying time results in significant changes in the temperature and velocity of the sprayed particles, resulting in significant changes in the coating structure and deposition efficiency [3,26]. Today, it is still not possible to predict the impact of electrode wear on the particle characteristics that would permit the operator to adjust the spray conditions to retrieve the appropriate temperature and velocity of the sprayed particles or to make a decision to stop the process and change the worn electrodes. In this context, the use of in-flight particle sensors is crucial to make the process more robust and reliable. Such sensors should be easy to use, relatively cheap, and give the necessary information to adjust the input spray parameters to keep the process under control (closed-loop feedback).

To address these needs, an ensemble particle jet diagnostic system was developed [15,16,27]. The system, the Accuraspray, is composed of a computer, CCD camera, analog signal processing unit, and an optical detection assembly made of a collecting lens, two optical fibers, filters, and photo-detectors as illustrated in Fig. 6. The thermal radiation emitted by the particle jet is collected by the two optical
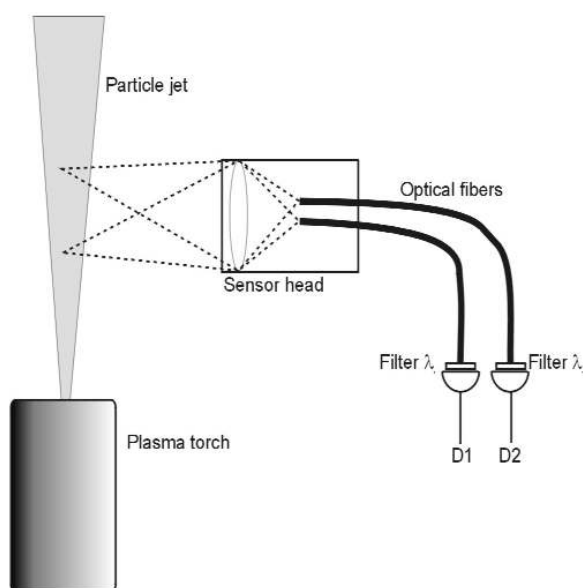
Fig. 6 Optical arrangement for measuring particle jet temperature and velocity as an ensemble in the Accuraspray sensor.

fibers whose diameter is 400 mm. The volume of measurement of each fiber is about $3 \times 3 \times 20$ mm^3 (optical magnification of 7.5) and is located in the middle of the particle jet. In typical spray conditions, the density of the spray particles in the jet ranges from 5 to 50 particles/cm^3 at normal stand-off distances. In these conditions, there are 1 to 10 particles seen simultaneously by each fiber. Figure 7a shows an example of signals detected by each detector. The passage of individual particles in the fiber field of view gives rise to characteristic light pulses as illustrated by the peaks in the figure.

The measurement of the mean temperature of the particle jet is obtained by two-color pyrometry after measuring the mean intensity of the fluctuations associated with the passage of the particles in each detector. The velocity measurement is obtained by evaluating the mean transit time for particles to move from the field of view of detector D_2 to that of detector D_1. As seen in Fig. 7a, many particles are detected first in D_2 and about 10 μs later in D_1. The mean transit time is obtained by calculating the cross-correlation between the two signals as given by eqs. 1 and 2 [28]:

$$\rho_{12} = \frac{\Gamma_{12}}{\sqrt{\Gamma_{11}\Gamma_{22}}} \tag{1}$$

where

$$\Gamma_{ij}(\tau) = \frac{1}{T}\int_0^T D_i(t)D_j(t+\tau)dt \tag{2}$$

where T is the acquisition period. Figure 7b shows the cross-correlation factor ρ_{12} as a function of the time delay τ calculated with the signals illustrated in Fig. 7a. The correlation is maximum when the time delay τ corresponds to the mean transit time of the particles. The mean velocity of the particle jet is thus calculated knowing the distance between the fibers and the optical magnification.

The orientation of the particle jet relative to the plasma torch axis as well as its width and total intensity are evaluated on-line from the analysis of images collected by the CCD camera. Both the camera and the optics for measuring the mean temperature and velocity are mounted rigidly in a single detection unit.
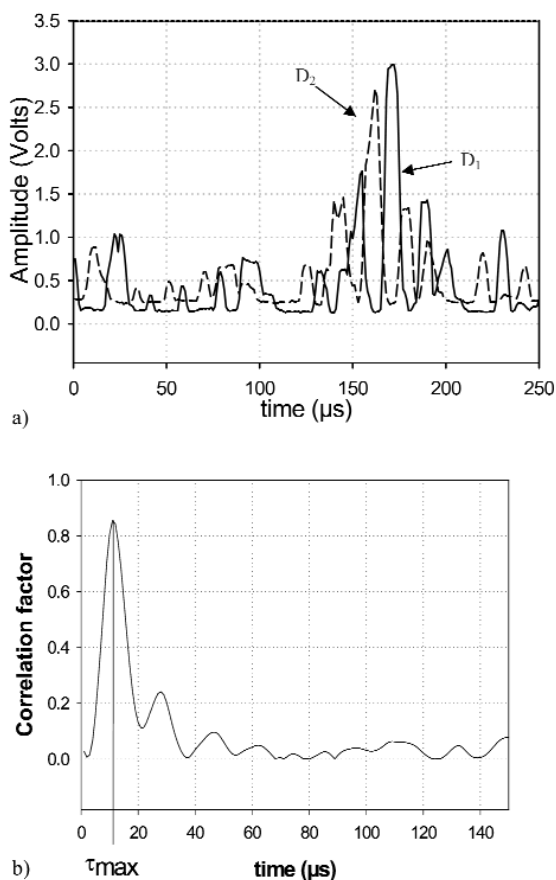
a)

b) τ_{max} time (µs)

Fig. 7 (a) Example of signals collected by the sensor head as a function of time and (b) the corresponding cross-correlation function. The delay τ_{max} corresponds to the mean time delay between the passages of the particles from detectors D_2 and D_1.

This approach for characterizing the plasma spray process has many advantages over the one used in the DPV-2000 unit for monitoring the process in a production environment. The time response of the system is much shorter using the correlation approach since hundreds of particles are analyzed simultaneously. Moreover, it can monitor high spray rate processes since the analysis of individual particles is not required.

As mentioned above, the control of the plasma spray process is very challenging, as many factors must be controlled. Using appropriate particle sensors makes it possible to detect any out-of-normal spray conditions and, eventually, adjust spray parameters to ensure constant particle conditions during spraying [29–31].

MONITORING PARTICLE IMPACTS ON A SUBSTRATE

The flattening and solidification of plasma-sprayed particles on a flat substrate are very complex phenomena difficult to study, as impact duration is of the order of 1 µs and the cooling rate of the sprayed droplets ranges from 10^6 to 10^8 K/s. Analytical and numerical models have been developed to better understand these rapid transient phenomena [32–34]. For example, the model developed by Madejski relates the flattening ratio (the ratio between the final splat diameter d and the initial droplet diameter

d_0) to the Reynold number Re, that is to say, to the velocity v, the density ρ, and viscosity μ of the impinging particle as given in eq. 3:

$$d\!\!\Big/\!\!d_0 = K\left(\text{Re}\right)^{0.2} = K\left(\frac{vd_0\rho}{\mu}\right)^{0.2} \tag{3}$$

where K is a constant. More recently, important efforts have been dedicated to develop a better understanding of the particle impact phenomena, both theoretically and experimentally [2,35–40]. Special efforts were dedicated to the study of the influence of the substrate temperature on particle flattening and solidification. It was shown that, on high-temperature substrates (around 300–400 °C), the sprayed particles tend to form well-shaped disks, while on room-temperature substrates, the splats tend to break in many droplets leading to the formation of distorted splats.

Figure 8 shows an example of an experimental set-up developed for monitoring particle impact on transparent and opaque substrates. The experimental set-up is similar to the one described previously in the literature [35], but an additional detector D_4 was placed behind the substrate to detect the thermal radiation emitted by the impacting particles at the same wavelength as detector D_2. A sensor head consisting of an achromatic lens, optical fiber, and optical mask located at the tip of the optical fiber collects radiation from the front surface of the substrate. The angle between the sensor head optical axis and the substrate surface is 30°. The collected radiation is transmitted to a detection box containing three detectors filtered at three different wavelengths. Detectors D_1 and D_2, filtered at 1000 and 790 nm, respectively, detect the thermal radiation emitted by the impacting particles. The particle temperature is determined from the ratio of the intensities of D_1 and D_2 (two-color pyrometry). A third detector D_3 is filtered at the wavelength of the laser diode (830 nm) used to illuminate the impact zone. The optical mask attached at the end of the optical fiber is composed of three transparent slits collecting radiation from the impinging particles in flight and upon impact on the substrate surface as illustrated in Fig. 9. A second sensor head, composed of a lens and optical fiber, collects the thermal radiation emitted by the impacting particles from the back of the substrate (for transparent substrates only). The angle between the optical axis of this sensor head and the substrate surface is 60°. The collected radiation is transmitted to the fourth detector D_4 filtered at the same wavelength as detector D_2 (790 nm).
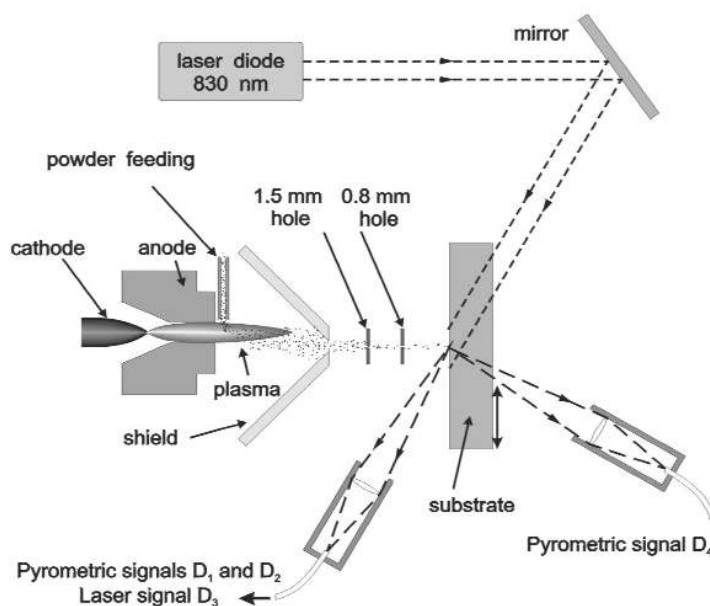

Fig. 8 Schema of the experimental set-up used for monitoring particle impacts on a transparent substrate.
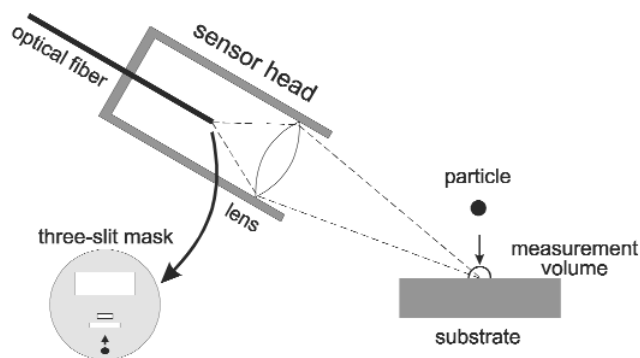
Fig. 9 Details of the sensor head optics. The three-slit mask is attached at the tip of the optical fiber.

For monitoring particle impacts, the plasma torch is swept in front of the experimental set-up. A very low powder feed rate is used to get zero or one particle impact per torch pass. If one particle is detected in the impact zone, the data acquisition system records signals detected by the four optical detectors and the collected data is saved on the hard disk of a personal computer. Figure 10 illustrates the field of view of the sensor head located in front of the substrate. A single particle is seen three times through the optical mask when it impinges on the substrate surface. The particle in-flight is seen first through the two small slits in positions b and c. The in-flight particle temperature, velocity and diameter are determined in a similar way as with the DPV-2000 system described above. When the particle reaches position f, it flattens and the amount of radiation collected increases as the particle surface area increases due to flattening. The evolution of the particle surface temperature (cooling rate) is obtained from the evolution of the ratio of the radiation intensity in detectors D_1 and D_2.

The laser beam illuminates the complete region seen through the third slit of the optical mask. When no particles are present in this impact region, intensity in D_3 is a maximum. The evolution of the particle size is obtained from attenuation of signal D_3 with time. As the particle flattens, its surface increases and intercepts a larger portion of the laser beam, giving rise to the attenuation of signal D_3.
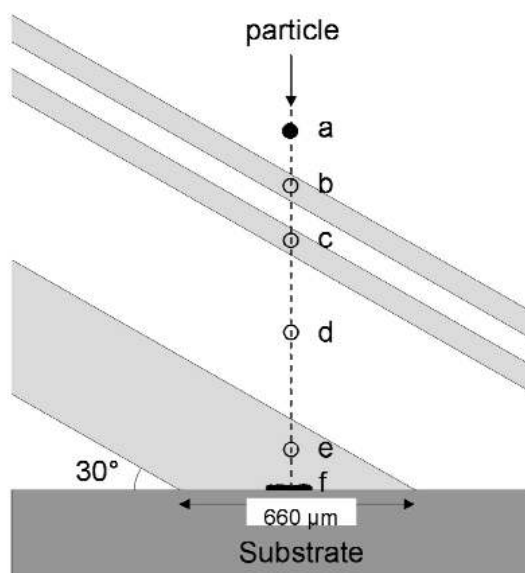

Fig. 10 Schema of the optical head field of view. The particles are seen first in flight through the first two slits of the optical mask (zones b and c) and then upon impact on the substrate (zones e and f).

Information about the evolution of the shape of the impacting particles is obtained from the ratio of signals D_2 and D_4. Indeed, as the two detectors are filtered at the same wavelength (790 nm) and see the same particle from different angles (30° and 60° for D_2 and D_4, respectively), the ratio D_2/D_4 depends on the actual shape of the particle. When the particle is still in flight just before its impact on the substrate, detectors D_2 and D_4 see it simultaneously (position e in Fig. 10). The shape of the particle at this position is a sphere so the particle surface area seen by both detectors is equal. At a later moment, if the particle forms a flat disk for example, the ratio D_2/D_4 will decrease by a factor 0.58 (sin 30°/sin 60°). If the ratio D_2/D_4 is normalized to one when the particle is in position e, its will decrease as the particle shape changes from a spherical form to a flat one. The temperature gradient across the particle thickness also influences the ratio D_2/D_4, as the thermal radiation intensity depends strongly on the temperature of the emitting surface.

Impacts on a hot glass substrate

Figure 11 shows an example of signals collected during the impact of a molybdenum particle on a glass substrate at 400 °C. Figure 11a shows the evolution of the two pyrometric signals D_1 and D_2. The two peak signals at $t = 3$ to 4 µs correspond to the passage of the in-flight particle in the field of view of the two small slits in the optical mask. At $t = 7$ to 8 µs, the in-flight particle enters the field of view of the third slit and then touches the substrate surface at $t = 10$ µs. About 2 µs later, the splat reaches its maximum extent and then the signals decrease as the temperature of the splat decreases rapidly. At 15 to 17 µsec, the signals reach a plateau corresponding to the solidification of the molybdenum splat. Figure 11b shows the corresponding evolution of the laser diode signal D_3. The signal is maximum before the
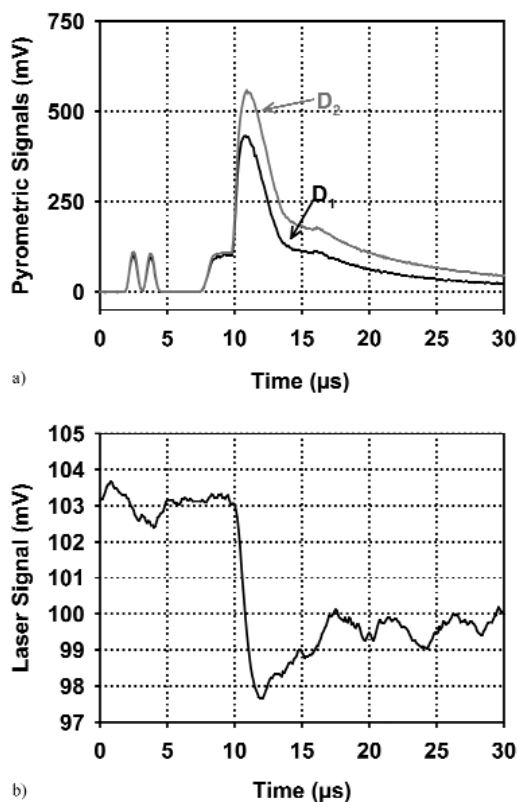

Fig. 11 (a) Evolution of the pyrometric signals D_1 and D_2 and (b) laser signal collected before and after a Mo particle impacts on a glass substrate at 400 °C.

impact of the particle, decreases rapidly as the splat extends, and then increases slightly. Figures 12a and 12b show the evolution of the surface temperature and equivalent diameter of the splat calculated from signals shown in Figs. 11a and 11b, respectively. One can see in Fig. 12a that the cooling rate of the splat is about 1.1×10^8 K/s during the first 3 to 4 μs after the impact. During this period, the metal is still liquid. Then a plateau that corresponds to the solidification of the liquid metal is clearly observed. The temperature is constant during this period because of the release of the latent heat of solidification. Once the solidification is finished, the temperature starts to decrease again, but at a lower rate. Figure 12b shows the evolution of the splat equivalent diameter calculated from the attenuation of the laser signal (Fig. 11b). One can see that the splat flattens rapidly during the first 2 μs and reaches a maximum diameter of about 170 mm. Then the splat contracts to a final diameter of about 140 mm. The contraction of the liquid splat is due to the surface tension of the molten molybdenum. The evolution of the ratio D_2/D_4 confirms that the shape of the particle changed from spherical to round as expected.
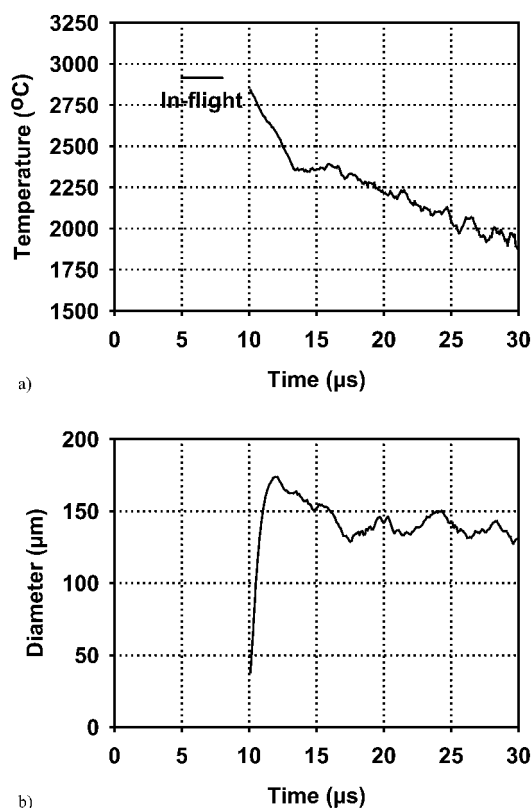

Fig. 12 Evolution of (a) the temperature and (b) equivalent diameter of a Mo particle impacting on a glass substrate at 400 °C as calculated from signals shown in Fig. 12.

Impacts on a cold glass substrate

The evolution of the temperature and equivalent diameter of a molybdenum particle on a glass substrate at room temperature is illustrated in Figs. 13a and 13b, respectively. Significant differences are observed in this case in comparison with results obtained on the hot substrate (Figs. 12a and 12b). Figure 13a shows that the cooling rate of the splat is about 5 times lower than that observed on the hot substrate (2.0×10^7 K/s instead of 1.1×10^8 K/s). This is an indication that the average quality of thermal contact between the splat and the substrate is poorer on the cold substrate. As shown in Fig. 13b, the evolution of the particle equivalent diameter is also significantly different on the cold substrate. One can
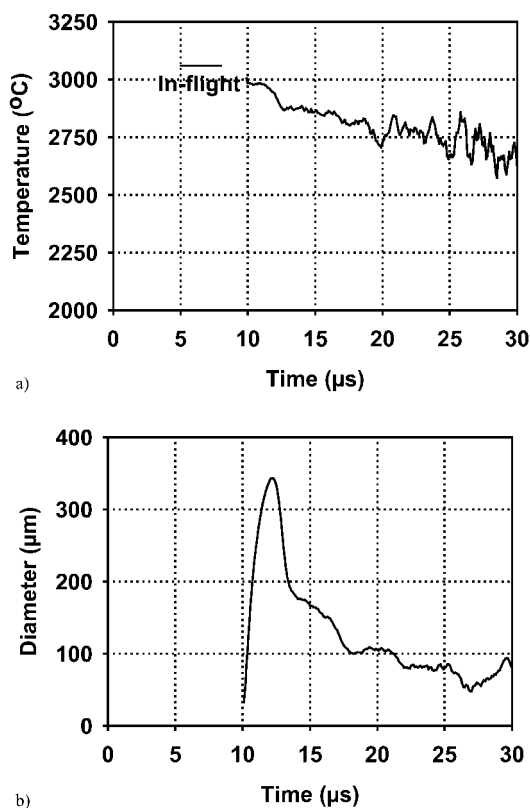
Fig. 13 Evolution of (a) the temperature and (b) equivalent diameter of a Mo particle impacting on a glass substrate at room temperature. As compared with Fig. 13 (400 °C), the particle cooling rate is much slower and the particle experienced a severe reduction of its surface area after reaching its maximum extent.

see that the maximum size of the splat reaches about 350 μm, which is about two times larger than that observed on the hot substrate. Moreover, after the maximum extent is reached after about 2 μs, the splat experienced a strong and rapid contraction that lasted for about 1 μs. After this rapid contraction period, a slower contraction is observed in the time period ranging from 13 to 25 μs. Analysis of the experimental results in different optical configurations shows that the rapid decrease of the equivalent splat diameter cannot be attributed to the exit of material outside the field of view of the sensor head.

One can observe in Fig. 13b that, in the region of maximum diameter ($t = 11–13$ μs), the magnitude of the slope during the rapid contraction period is higher than the slope during the flattening period. This is an indication that the contraction is not only due to the contraction of the liquid disk of molten metal since, in that case, the contraction would be slower than the initial expansion (flattening) of the splat as kinetic energy is dissipated owing to the finite viscosity of the molten metal. One concludes that the thin metal film that exists for 1 μs or so breaks into many segments that contract under surface tension. The thin metal film of about 350 μm in diameter and 0.5 μm thick is very unstable and breaks, leaving debris on the substrate around the impact point of the impinging particle [35]. The change of shape of the splat during the rapid contraction period is confirmed by the evolution of the ratio D_2/D_4, as shown in Fig. 14. One can see that upon impact at $t = 10$ μs, the shape of the particle changes from a sphere to a disk as expected. However, at $t = 12–13$ μs, the shape factor increases, indicating that the splat comes back to a partially spherical shape. This shape change occurs simultaneously with the rapid contraction of the splat shown in Fig. 13b.
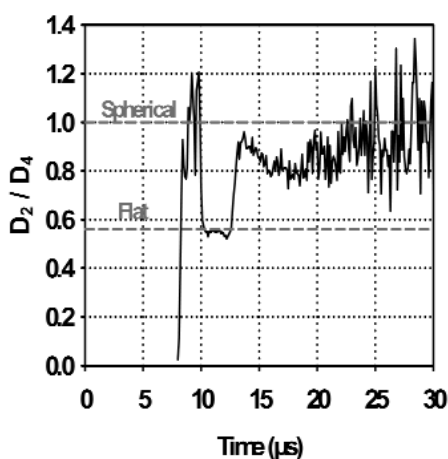
Fig. 14 Evolution of the shape factor D_2/D_4 as a function of time. The particle was spherical in flight, became flat for a few microseconds ($t = 10–13$ μs) upon impact, and came back to a mostly spherical form during the rapid contraction occurring at $t = 13$ μs as shown in Fig. 13b.

As stated above, the influence of the substrate temperature is a key parameter influencing the structure and properties of the coatings. The experimental set-up developed for monitoring the particle impacts is a tool that makes possible the development of a better understanding of the extremely rapid physical transformations occurring during impact of particles under plasma spray conditions.

OPTIMIZATION OF NANOSTRUCTURED PLASMA-SPRAYED COATINGS

Plasma spraying of nanostructured materials is a challenge. The maximum temperature of a plasma jet may reach values up to 20 000 °C [41]. Owing to the high temperatures associated with the plasma spray, this process is employed worldwide to spray ceramic materials, which generally exhibit high melting points. Complete particle melting via plasma spray is the traditional approach to produce conventional ceramic coatings. For nanostructured materials, it is paramount to retain some of the pre-existing nanostructure of the feedstock in order to produce coatings with nanostructure-related properties. If the nanostructured feedstock particles are fully melted during spraying, all the original nanostructured features will be destroyed and the coating will tend to behave as one produced using a conventional feedstock [42,43]. However, due to the lack of plasticity of ceramic materials, it is necessary to have some degree of particle melting in order to promote the necessary physical conditions for particle/coating cohesion and adhesion. Consequently, by controlling the percentage of fully molten and semi-molten nanostructured particles incorporated into the coating microstructure, it is possible to engineer nanostructured thermal spray coatings with distinct properties [42,43].

Owing to the characteristics described above, an in-flight particle diagnostic system is a key tool for identifying and controlling suitable spray conditions by monitoring particle temperature, velocity, and diameter in the plasma jet. Such an approach was used for producing nanostructured titania coatings by plasma spraying. A nanostructured titania feedstock (Altair Nanomaterials, Reno, NV) was air plasma sprayed and, based on particle temperature distributions in the plasma jet analyzed using the DPV-2000, two main sets of spray parameters (high- and low-temperature) were selected for producing coatings. The effect of these parameter sets on both the in-flight particle characteristics and on the deposited coating will be discussed below.

Figure 15 shows the polished cross-section of a typical agglomerated nanostructured titania feedstock particle. Individual nanoparticles cannot be successfully deposited by thermal spray because of their low mass. They do not have the inertia necessary to cross the streamlines in the spray jet and tend
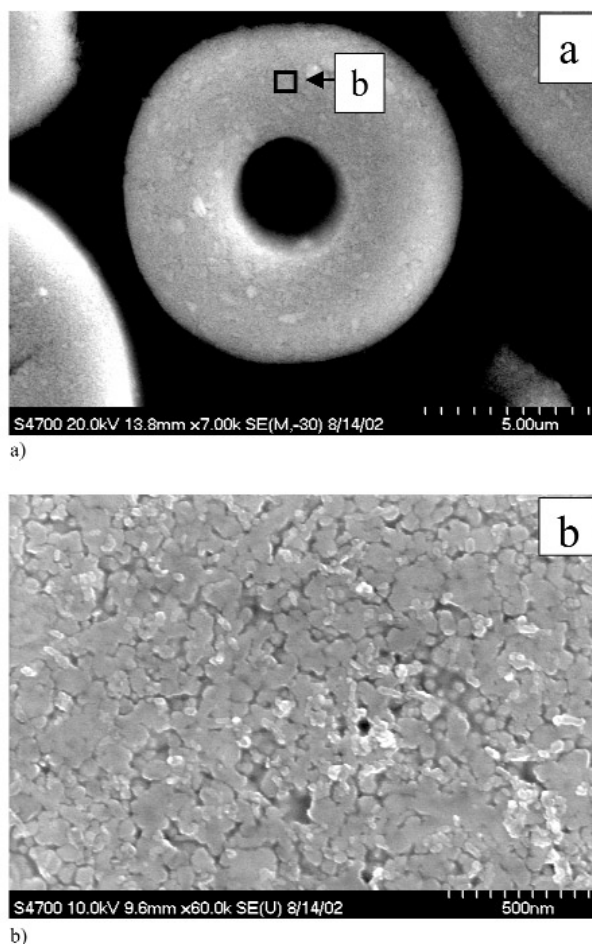
Fig. 15 (a) Typical morphology of a nanostructured titania feedstock particle. The nanostructured nature of the particle is clearly visible in micrograph (b) taken at higher magnification.

to be segregated to its periphery failing to deposit on the substrate. To overcome this problem, microscopic feedstock particles are typically produced by an agglomeration (spray-drying) of individual nanosized particles, as observed in Fig. 15.

Plasma spraying the nanostructured feedstock employing high- and low-temperature conditions leads to the formation of different percentages of molten and semi-molten particles. Since a certain fraction these particles are deposited on the substrate to produce a coating, these differences in the degree of melting would be reflected in the coating microstructure. In this work, the melting point of titania (1855 °C [44]) was taken as a reference for evaluating the degree of particle melting. It was assumed that particles that exhibited superficial temperatures close to 1855 °C would be semi-molten, whereas particles exhibiting superficial temperatures well above the melting point of titania would be fully molten.

In order to quantify of the degree of melting of the in-flight particles, a total of 3000 particles were analyzed with the DPV-2000 for each set of spray parameters. The in-flight particle data were acquired at a spray distance of 10 cm (the distance at which the substrate would normally be positioned when depositing a coating). The average particle velocity and standard deviation for the low- and high-temperature conditions were 245 ± 43 m/s and 327 ± 143 m/s, respectively. The average and

standard deviation values of particle temperature for the low- and high-temperature conditions were 2065 ± 270 °C and 2551 ± 308 °C, respectively.

As previously stated, controlling the particle temperature is a very important issue when thermal spraying nanostructured materials. For this reason, the overall distribution of particle temperature for the low- and high-temperature conditions were analyzed, as shown in Figs. 16 and 17, respectively. It is observed that for the high-temperature condition (Fig. 17) the majority of the particles (in number) have surface temperatures above that of the melting point of the titania. As already mentioned, it is thought that the particles that exhibit temperatures around the melting point of titania are partially molten particles, whereas the particles exhibiting temperatures well above the melting point represent the fully molten particles. In order to have more representative data of the process using particle volume rather than particle number, the total volume of the sprayed particles was calculated and the percentage of particles (in volume) exhibiting superficial temperatures above the melting point of titania was determined. For the low- (Fig. 16) and high- (Fig. 17) temperature conditions used with the nanostructured feedstock, the percentages in volume of the particles that exhibited temperatures above the melting point of titania were 46 and 87 %, respectively. Consequently, it was assumed that for the high-temperature condition the majority of the sprayed particles would be fully molten, while for the low-temperature condition the percentage of semi-molten particles embedded in the coating microstructure would tend to be higher.
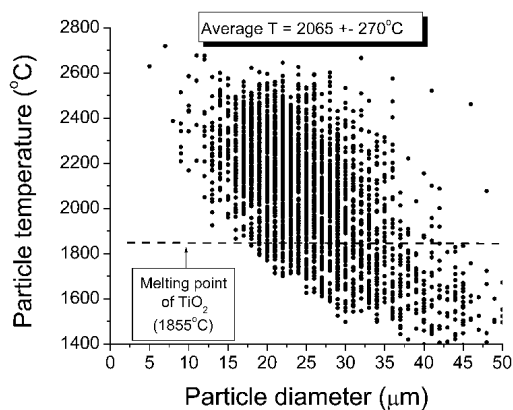

Fig. 16 Particle temperature vs. diameter for the low-temperature-condition set.
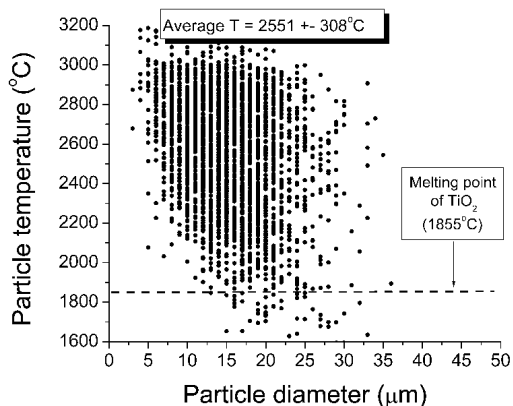

Fig. 17 Particle temperature vs. diameter for the high-temperature-condition set.

The mechanical behavior of coatings produced using these two sets of spray conditions was compared using indentation technique. A total of 5–10 Vickers indentation tests were performed under a 5 kgf load for 15 s on the polished cross-section of each coating. The indentations were positioned near the centerline of the coating thickness and the orientation of the indenter was selected so that one diagonal of the Vickers indentation impression was parallel to the substrate surface. Figures 18 and 19 show the typical indentation impression and crack propagation characteristics for the two titania coatings (the horizontal crack is parallel to the substrate surface).
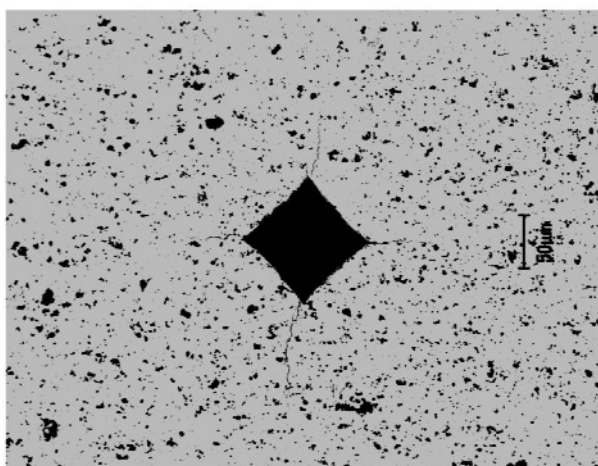

Fig. 18 Vickers indentation impression for the nanostructured titania coating sprayed using low-temperature conditions.
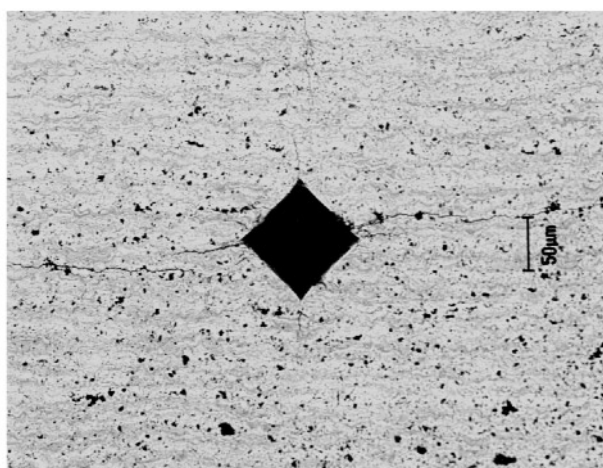

Fig. 19 Vickers indentation impression for the nanostructured titania coating sprayed using high-temperature conditions.

The average and standard deviation values for the cracks parallel to the substrate surface for the titania coatings (low- and high-temperature conditions) were 219 ± 18 µm and 678 ± 31 µm, respectively. Therefore, the nanostructured titania coating sprayed using low-temperature conditions, which had the lowest percentage in volume (46 %) of particles having their temperatures above the melting point of titania, exhibited the highest resistance to delamination under indentation.

It is interesting to observe that the regular layered microstructure of ceramic thermal spray coatings is not clearly observed for the titania coating sprayed using the low-temperature-condition set (Fig. 18), whereas for the high-temperature condition (Fig. 19), the typical layered thermal spray microstructure originating from the impact and spreading of fully molten particles is more readily observed.

The deposition efficiency (DE) values are also in line with the results of the DPV-2000 (Figs. 16 and 17) and the microstructural characteristics (Figs. 18 and 19) of the coatings. For the low-temperature-condition set the DE was ~40 %, whereas for the high-temperature-condition set the DE was ~67 %. The higher amount of fully molten particles in the high-temperature condition increased the DE values; however, this coating exhibited a lower resistance to delamination under indentation (Fig. 19).

Figure 20 shows the fracture surface of the nanostructured titania coating sprayed using the low-temperature condition. It is possible to observe that part of the original nanostructure of the feedstock (Fig. 15) is preserved in the coating microstructure. This illustrates how important a role monitoring of the in-flight characteristics of sprayed particles can play in identifying the conditions required to preserve the nanostructure of the feedstock in order to produce coatings with superior properties.
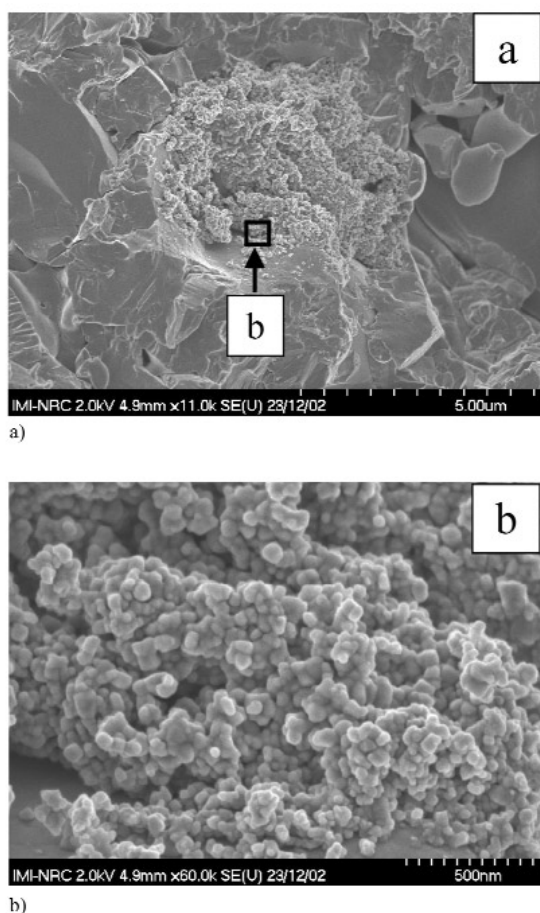

Fig. 20 (a) Fracture surface of the nanostructured titania coating sprayed using low-temperature conditions. The nanostructure is preserved in some locations as shown in micrograph (b) taken at higher magnification.

CONCLUSION

In this paper, a few examples of advanced diagnostic techniques for monitoring and controlling plasma spray processes have been presented. Such tools have been used and will continue to be used for developing a better understanding of all steps involved in the deposition of materials. Particle diagnostics are particularly important since coating properties depend closely on the temperature and velocity of the particles during spraying. By better controlling these characteristics as well as substrate temperature, one can tailor specific coating properties to meet the requirements of the applications in which they will be used.

These diagnostic tools are not only useful for the scientists, but they will become more and more important for engineers on the production floor. Indeed, coatings are used in increasingly demanding applications requiring not only optimum coating performance, but also a high degree of consistency. For example, prime-reliant thermal barrier coatings are required in land-based turbines. A failure in the coating system would lead to rapid turbine degradation. So, in this context, coatings have to be deposited in a reproducible manner day after day. Establishing a control strategy based only on the monitoring and control of input spray parameters is not sufficient to reach this level of consistency. Rugged and easy-to-use sensors monitoring the state of the particle jet will provide the necessary source of data for better controlling the plasma spray process enabling an increase in the current level of reproducibility of the process.

REFERENCES

1. L. Pawlowski. *The Science and Engineering of Thermal Spray Coatings*, John Wiley, New York (1995).
2. P. Fauchais, A. Vardelle, B. Dussoubs. *J. Therm. Spray Technol.* **10**, 44–66 (2001).
3. L. Leblanc and C. Moreau. *J. Therm. Spray Technol.* **11**, 380–386 (2002).
4. P. Gougeon, C. Moreau, F. Richard. In *Advances in Thermal Spray Science and Technology*, C. C. Berndt and S. Sampath (Eds.), pp. 149–155, Proc. National Thermal Spray Conference 1995, Houston, Texas, ASM International, Materials Park, OH (1995).
5. M. Vardelle, A. Vardelle, P. Fauchais, K.-I. Li, B. Dussoubs, N. J. Themelis. *J. Therm. Spray Technol.* **10**, 267–284 (2001).
6. C. Moreau. In *Thermal Spray: Meeting the Challenges of the 21st Century*, C. Coddet (Ed.), pp. 1681–1693, Proc. 15th Int. Thermal Spray Conference 1998, Nice, France, ASM International, Materials Park, OH (1998).
7. M. Friis and C. Persson. *J. Therm. Spray Technol.* **12**, 44–52 (2003).
8. J. Mishin, M. Vardelle, J. Lesinski, P. Fauchais. *J. Phys. E: Sci. Instrum.* **20**, 620–625 (1987).
9. M. Vardelle, A. Vardelle, P. Fauchais, M. I. Boulos. *AIChE J.* **29**, 236–243 (1983).
10. J. Fincke, C. L. Jeffery, S. B. Englert. *J. Phys. E: Sci. Instrum.* **21**, 367 (1988).
11. J. Fincke, W. D. Swank, C. K. Jeffery, C. A. Mancuso. *Meas. Sci. Technol.* **4**, 449–565 (1993).
12. S. Coulombe and M. I. Boulos. *Plasma Chem. Plasma Process.* **15**, 653–675 (1995).
13. V. P. Lyagushkin and O. P. Solonenko. *Symp. Proc.–Int. Symp. Plasma Chem.* 7, paper B-5-5, p. 730, Eindhoven (1985).
14. J. Blain, F. Nadeau, L. Pouliot, C. Moreau, P. Gougeon, L. Leblanc. *Surf. Eng.* **13**, 420–424 (1997).
15. G. Bourque, M. Lamontagne, C. Moreau. In *Surface Engineering via Applied Research*, C. Berndt (Ed.), pp. 45–50, Proc. Int. Thermal Spray Conference 2000, Montreal, Canada, ASM International, Materials Park, OH (2000).
16. Tecnar Automation Ltée, 1321 Hocquart, St-Bruno, Québec, Canada, J3V 6B5.
17. J. Vattulainen, E. Hämäläinen, R. Hernberg, P. Vuoristo, T. Mäntylä. *J. Therm. Spray Technol.* **10**, 94–104 (2001).

18. Oseir Ltd., Hermiankatu 6°, FIN-33720, Tampere, Finland.

19. J. E. Craig, R. A. Parker, D. Y. Lee, T. Wakeman, J. Heberlein, D. Guru. In *Thermal Spray 2003: Advancing the Science and Applying the Technology*, B. R. Marple and C. Moreau (Eds.), pp. 1107–1112, Proc. Int. Thermal Spray Conference 2003, Orlando, Florida, ASM International, Materials Park, OH (2003).

20. Stratonics, Inc., 23151 Verdugo Dr. #114 Laguna Hills, CA, USA, 92653.

21. C. Moreau, P. Gougeon, M. Lamontagne, V. Lacasse, G. Vaudreuil, P. Cielo. In *Thermal Spray Industrial Applications*, C. C. Berndt and S. Sampath (Eds.), pp. 431–437, Proc. Nat. Therm. Spray Conf. 1994, Boston, MA, ASM International, Materials Park, OH (1994).

22. J. F. Bisson, B. Gauthier, C. Moreau. *J. Therm. Spray Technol*. **12**, 38–43 (2003).

23. J. F. Bisson and C. Moreau. *J. Therm. Spray Technol*. **12**, 258–264 (2003).

24. Z. Duan and J. Heberlei. In *Thermal Spray: Surface Engineering via Applied Research*, C. C. Berndt (Ed.), pp. 1–7, Proc. Int. Therm. Spray Conf. 2000, Montreal, Canada, ASM International, Materials Park, OH (2000).

25. S. Wutzke, E. Pfender, E. Eckert. *AIAA J*. **5**, 1216–1232 (1967).

26. L. Leblanc, P. Gougeon, C. Moreau. In *Thermal Spray: A United Forum for Scientific and Technological Advances*, C. Berndt (Ed.), pp. 567–575, Proc. 1st United Therm. Spray Conf. 1997, Indianapolis, Indiana, ASM International, Materials Park, OH (1997).

27. J. F. Bisson, C. Moreau, L. Pouliot, J. Blain, F. Nadeau. In *Thermal Spray 2001*, C. Berndt, K. A. Khor, E. F. Lugscheider (Eds.), pp. 705–714, Proc. Int. Therm. Spray Conf. 2001, Singapore, ASM International, Materials Park, OH (2001).

28. M. S. Beck and A. Plaskowski. *Cross-Correlation Flowmeter: Their Design and Application*, Adam Hilger, Bristol (1987).

29. J. R. Fincke, W. D. Swank, R. L. Bewley, D. C. Haggard, M. Gevelber, D. Wroblewski. *Surf. Coat. Technol*. **146–147**, 537–543 (2001).

30. J. R. Fincke, W. D. Swank, R. L. Bewley, D. C. Haggard, M. Gevelber, D. Wroblewski. In *Thermal Spray 2003: Advancing the Science and Applying the Technology*, B. R. Marple and C. Moreau (Eds.), pp. 1093–1099, Proc. Int. Thermal Spray Conference 2003, Orlando, Florida, ASM International, Materials Park, OH (2003).

31. J. Blain, L. Pouliot, F. Nadeau, J.-F. Bisson, G. Vaudreuil, C. Moreau. In *Thermal Spray 2003: Advancing the Science and Applying the Technology*, B. R. Marple and C. Moreau (Eds.), pp. 1131–1138, Proc. Int. Thermal Spray Conference 2003, Orlando, Florida, ASM International, Materials Park, OH (2003).

32. J. Madejski. *Int. J. Heat Mass Transfer* **19**, 1009–1013 (1976).

33. J. Madejski. *Int. J. Heat Mass Transfer* **26**, 1095–1098 (1983).

34. J. Mostaghimi, M. Pasandideh-Fard, S. Chandra. *Plasma Chem. Plasma Process.* **22**, 59–84 (2002).

35. P. Gougeon and C. Moreau. *J. Therm. Spray Technol.* **10**, 76–82 (2001).

36. M. Fukumoto, E. Nishiokam, T. Nishiyama. *Surf. Coat. Technol.* **161**, 103–110 (2002).

37. M. Fukumoto, E. Nishiokam, T. Nishiyama. *Surf. Coat. Technol.* **120–121**, 131–137 (1999).

38. X. Jiang, Y. Wan, H. Herman, S. Sampath. *Thin Solid Films* **385**, 132–141 (2001).

39. C. Escure, M. Vardelle, P. Fauchais. *Plasma Chem. Plasma Process.* **23**, 185–221 (2003).

40. L. Bianchi, A. C. Leger, M. Vardelle, A. Vardelle, P. Fauchais. *Thin Solid Films* **305**, 35–47 (1997).

41. E. Pfender. *Surf. Coat. Technol.* **34**, 1–14 (1988).

42. R. S. Lima, A. Kucuk, C. C. Berndt. *Mater. Sci. Eng. A* **313**, 75–82 (2001).

43. R. S. Lima, A. Kucuk, C. C. Berndt. *Mater. Sci. Eng. A* **327**, 224–232 (2002).

44. M. Miyayama, K. Koumoto, H. Yanagida. In *Engineered Materials Handbook*, Vol. 4 – *Ceramic and Glasses*, S. J. Schneider (Ed.), pp. 748–757, ASM International, Materials Park, OH (1991).